Synthesis and Characterization of the Novel Antiferromagnet $LaNiB_3O_7$

Kelly M. Powderly,[a,*] Shu Guo,[a] Karoline Stolze,[a†] Elizabeth M. Carnicom,[a] and R. J. Cava[a,*]

[a]Department of Chemistry, Princeton University, Princeton, New Jersey 08544, USA

Abstract

We present the synthesis, structure, and magnetic properties of the novel borate $LaNiB_3O_7$ – the first magnetically ordered compound reported in the $CaAlB_3O_7$ structure type. The material is made of alternating sheets of corner-sharing borate tetrahedra and planes of La and Ni ions, with distorted nickel oxide [NiO_6] octahedra and lanthanum oxide [LaO_{10}] polyhedra. Temperature-dependent magnetic susceptibility measurements reveal dominantly antiferromagnetic interactions and an antiferromagnetic transition with a Néel temperature of 19 K, confirmed by specific heat data. The magnetic moment per nickel ion is 2.66 μ_B. This compound uncovers a new family of rare-earth transition-metal borates to probe for magnetic interactions.

Keywords: Borate, nickel, antiferromagnetic, single crystal X-ray diffraction, magnetism

---

† Present address: Leibniz Institute for Crystal Growth, Forschungsverbund Berlin e.V., Max-Born-Str. 2, D-12489 Berlin, Germany

*Corresponding author(s).

E-mail addresses: powderly@princeton.edu (K.M. Powderly), rcava@princeton.edu (R.J. Cava)

1. Introduction

Borate compounds that contain rare-earth (*RE*) and transition metal (*TM*) ions are of interest due to their potential for displaying interesting optical and magnetic properties. For example, hexagonal La_3BWO_9, with its non-centrosymmetric structure, exhibits second-harmonic generation and non-linear optical properties[1,2] while isomorphous Eu_3BWO_9 is a red-emitting phosphor[3]. Within a different complex borate structure type, the *RE* iron borate $LaFe_3(BO_3)_4$ orders antiferromagnetically with a Néel temperature (T_N) of 23 K[4,5]. Other isostructural $LnFe_3(BO_3)_4$ compounds – *Ln*= Y, Ce-Nd, Sm-Ho – also exhibit antiferromagnetism, with Néel temperatures up to 40 K[5–9]. Interestingly, the layered perovskites $YCr(BO_3)_2$ and $HoCr(BO_3)_2$ display magnetodielectric coupling and canted antiferromagnetism[10,11]. Considering the rich structural chemistry offered by the *RE*- and *TM*-based quaternary borates, the synthesis of new phases with structures previously unstudied in this class of materials may reveal additional exotic properties.

Here we report the synthesis, structure determination, and magnetic characterization of $LaNiB_3O_7$. To the best of our knowledge, this tan compound is the third reported with the $CaAlB_3O_7$ structure type[12] and the first in this structure type to contain a transition metal or exhibit magnetic ordering. The compound displays antiferromagnetic ordering with a Néel temperature of 19 K, as determined by magnetic susceptibility measurements and confirmed by temperature-dependent specific heat.

2. Materials and Methods

2.1 Synthetic Methods

Polycrystalline samples of $LaNiB_3O_7$ were synthesized by combining powders of $La(NO_3)_3{\bullet}6H_2O$ (0.2462 mmol, Johnson Matthey Catalog Co., 99.9%), $NiCO_3$ (0.2468 mmol, Alfa

Aesar, 99%), and B_2O_3 (0.9221 mmol, Alfa Aesar), with excess B_2O_3 to account for loss through volatilization. The sample was first annealed in air in an alumina crucible at 700 °C to decompose the nitrate and carbonate precursors, then quenched to room temperature, and ground. The sample was then placed in an alumina crucible and heated to 850 °C at a rate of 3°/min under flowing O_2, dwelling at temperature for 2 days, then cooled at the same rate.

2.2 Structural Characterization

Single crystal X-ray diffraction (sXRD) data were obtained at 299(1) K with a Kappa Apex2 CCD diffractometer (Bruker) using graphite-monochromated Mo-Kα radiation (λ = 0.71073 Å). A small crystal from the polycrystalline sample was mounted on a goniometer head in paratone-N oil. The raw data were corrected for background, polarization, and the Lorentz factor. Multi-scan absorption corrections were also applied. Finally, the structure was analyzed by the Intrinsic Phasing method provided by the ShelXT structure solution program and refined using the ShelXL least-squares refinement package[13] with the Olex2 program[14]. The ADDSYM algorithm in the program PLATON was used to double check for possible higher symmetry[15].

Powder X-ray diffraction (pXRD) data were collected using the Bruker D8 Advance Eco with Cu Kα radiation (λ = 1.5406 Å) and a LynxEye-XE detector at room temperature. A thin layer of sample powder was held to a glass disk using Dow Corning high vacuum grease. Data suitable for a Rietveld Refinement were collected over 180 minutes with rotation, from 5.062° to 110.002° 2θ with a step size of 0.0103°. A Rietveld refinement of the phases present was performed in the FullProf Suite using Thompson-Cox-Hastings pseudo-Voigt peak shapes, using the results from the single crystal refinement as a starting point. The Rietveld refinement is consistent with the

single crystal refinement and thus only the single crystal refinement results will be discussed here. The program VESTA was used for all crystal structure images[16].

2.3 Room-temperature Resistance

A room-temperature two-probe resistance measurement on a pressed and annealed pellet (1.87×1.47×0.25 mm^3) showed that $LaNiB_3O_7$ is highly insulating, with a resistance value at or above 2 MΩ. This confirms that the compound is an insulator, as expected since the sample is tan in color.

2.4 Magnetic Characterization

Magnetization measurements were performed with the Quantum Design Physical Property Measurement System (PPMS) Dynacool with the vibrating sample magnetometer (VSM) option. The polycrystalline samples were placed in a plastic sample container and mounted in a brass sample holder. Zero-field-cooled (ZFC) temperature-dependent dc magnetization (M) was measured in the temperature range of 1.74 K to 300 K in applied fields (H) of 5000 Oe and 3000 Oe. Susceptibility is defined here as $\chi = \Delta M/\Delta H$. Inverse magnetic susceptibility plots were fit in the linear region, from 50 to 280 K, using the Curie-Weiss law,

$$\chi - \chi_0 = \frac{C}{T - \theta_{CW}}$$

where χ is the magnetic susceptibility, χ_0 is the temperature independent factor dominantly from core diamagnetism in electronic insulators such as this material, C is the Curie constant, and θ_{CW} is the Weiss temperature. The effective magnetic moment (μ_{eff}) per nickel atom was determined from C using the following equation:

$$\frac{\square_{eff}}{\square\square} = \frac{\sqrt{8\square}}{1\ \square\square\square\ \square\square/\square.\square.}$$

where f.u. is formula unit and $\square_{eff}$ is in units of Bohr magnetons ($\square_{\square}$).

Magnetization versus applied field measurements were also performed at various temperatures up to 5000 Oe and down to -5000 Oe, at a sweep rate of 7 Oe/s.

2.5 Specific Heat Measurements

Specific heat data were collected with the Quantum Design PPMS Dynacool using a two-tau relaxation method. The polycrystalline $LaNiB_3O_7$ powder was pressed in a ~1/8"-thin pellet and annealed at 200 °C for 12 hours. An addenda-subtracted data collection was performed from 1.85 to 40 K under zero applied magnetic field.

3. Results and Discussion

The previously unreported compound $LaNiB_3O_7$ was synthesized as a polycrystalline sample from the decomposed lanthanum nitrate and nickel carbonate precursors, as it could not be synthesized with high purity from supplier-provided oxide reactants. As determined from collection and analysis of sXRD data, $LaNiB_3O_7$ was found to crystallize in the space group *Cmme*, with lattice parameters a = 8.0367(2) Å, b = 11.8464(3) Å, and c = 4.5927(1) Å. A summary of the single crystal refinement results is shown in **Table 1** and atomic coordinates in **Table 2**. We searched the Inorganic Crystal Structure Database (ICSD) [12] and found that our phase matches well with the $CaAlB_3O_7$ structure type. Two previous phases are known to crystallize in this structure type: its namesake mineral $CaAlB_3O_7$, also called Johachidolite [17–19], and β-$SrAl_4O_7$ [20].

Table 1

Crystal data and ambient temperature single crystal structure refinements for $LaNiB_3O_7$.

Formula	$LaNiB_3O_7$
formula mass(amu)	342.05
Crystal system	orthorhombic
space group	*Cmme*
a(Å)	8.0367(2)
b(Å)	11.8464(3)
c(Å)	4.59270(10)
V(Å^3)	437.252(18)
Z	4
T(K)	299(1)
ρ*(calcd)(g/cm^3)*	5.196
λ (Å)	0.71073
F(000)	624
θ*(deg)*	3.44 - 36.40
Cryst size (mm^3)	0.075 × 0.049 × 0.04
μ(mm^{-1})	13.921
R_1*(obs)*	0.0117
R_1*(all Fo)*	0.0311
R_2*(all Fo)*	0.0328
Residual electron density	-0.982
/ (eÅ^{-3})	0.162
Goodness of fit (GooF)	1.107

Table 2

Wyckoff positions, coordinates, occupancies, and equivalent isotropic displacement parameters for $LaNiB_3O_7$.

Atoms	Wyck.Site	*x*	*y*	*z*	S.O.F.	U_{eq}
La1	4*f*	0.25	0.25	0.5	1	0.00535(5)
Ni1	4*d*	0	0	0.5	1	0.00419(7)
O1	8*m*	0	0.63934(12)	0.2653(3)	1	0.0052(2)
O2	4*g*	0	0.25	0.1744(5)	1	0.0049(3)
O3	16*o*	0.14760(12)	0.07565(8)	0.1839(2)	1	0.00468(16)
B1	4*a*	0.25	0	0	1	0.0036(4)
B2	8*m*	0	0.13501(19)	0.0392(4)	1	0.0047(4)

$LaNiB_3O_7$ is made up of layers of corner-sharing $[BO_4]$ tetrahedra arranged in 6-membered and 4-membered rings, as shown in **Fig. 1a**. Coplanar La^{3+} and Ni^{2+} ions reside in the space between these borate sheets, lined up within the channels formed by the 6-membered and 4-membered rings, respectively (**Fig. 1b**). Based on the interatomic distances from the La and Ni atoms to the oxygen atoms, the shortest being 2.505(2) and 1.972(2) Å respectively, the borate sheets can be considered as bonded to one another by these ions rather than truly layered. In fact, the units formed by the four-membered rings of borate tetrahedra and nickel-oxide octahedra can be described as infinite columns of composition $[NiB_4O_{12}]^{10-}$, analogous to the $[AlB_4O_{12}]^{9-}$ columns found in $CaAlB_3O_7$**Error! Bookmark not defined.**.

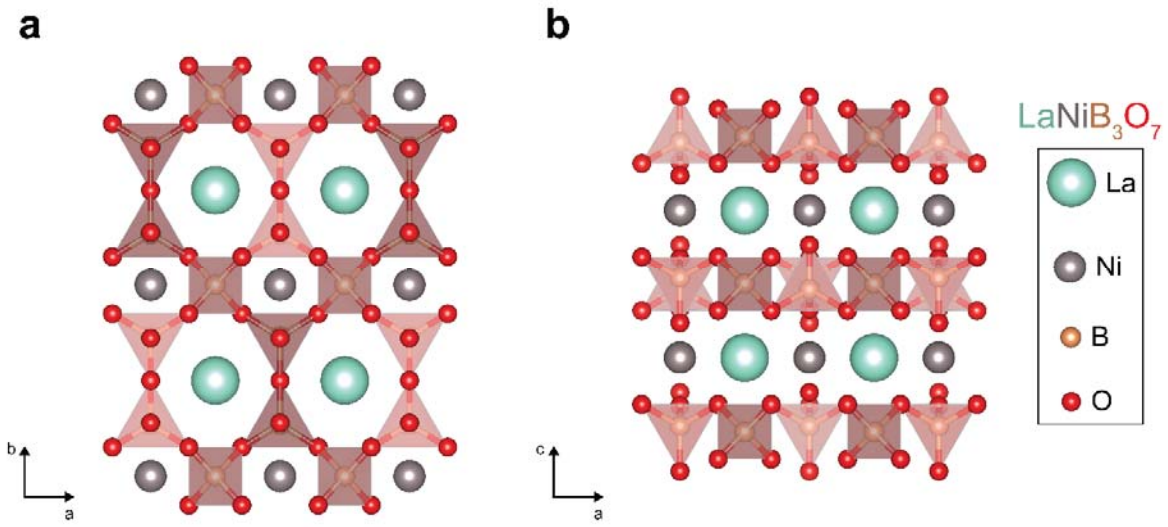

Fig. 1. Crystal structure of $LaNiB_3O_7$: (a) along the *c*-axis, emphasizing the framework of borate tetrahedra and position of the metal atoms in the channels, and (b) along the *b*-axis, depicting the alternating sheets of borate tetrahedra and coplanar La and Ni ions. La is shown in blue, Ni in gray, B in orange, and O in red.

In this structure, the nickel atoms are 6-fold coordinated by oxygen in distorted NiO_6 octahedra, which tilt in alternating directions within the structure (**Fig. 2a**). The angles of the O–Ni–O bonds are substantially offset from the ideal 90°, with values of 110.38(6)° and 69.62(6)° between the equatorial Ni–O bonds and 88.80(5)° and 91.20(5)° between the axial and equatorial bonds (**Fig. 2b**). The octahedra display an elongation of the four equatorial Ni–O bonds, at 2.078(1) Å, and a contraction of the two axial Ni–O bonds, at 1.972(2) Å (**Fig. 2c**). The lanthanum atoms are 10-fold coordinated by oxygen in a pentagonal antiprism. This polyhedron is irregular, with La–O bond distances of 2.505(2), 2.655(1), 2.655(1), 2.630(1), and 2.630(1) Å and O–La–O angles of 120.23(5), 104.96(5), 104.96(5), 104.79(4), and 104.79(4)° for each pentagonal face.

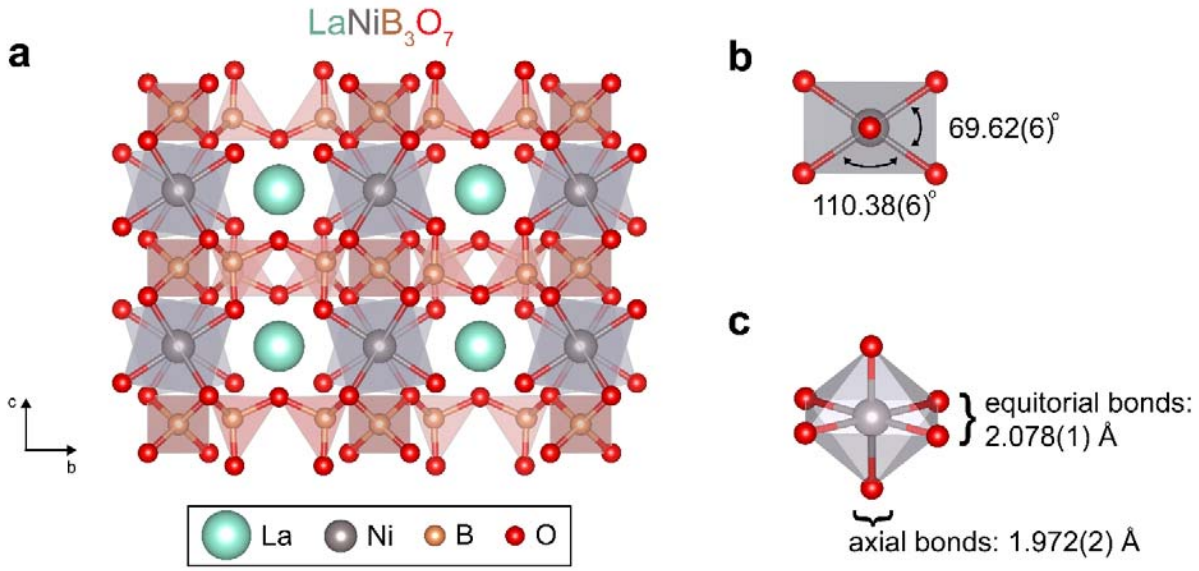

Fig. 2. (a) Crystal structure of $LaNiB_3O_7$ along the *a*-axis, showing the staggered arrangement of the tilted nickel-oxide octahedra; these octahedra are highly distorted (b) in bond angles, with equatorial O–Ni–O angles of 69.62(6)° and 110.38(6)° instead of the ideal 90°, and (c) in bond lengths, with the equatorial Ni–O bonds being longer than the axial bonds, 2.078(1) Å vs. 1.972(2) Å respectively. La is shown in blue, Ni in gray, B in orange, and O in red.

Starting from the unit cell symmetry and parameters obtained from the sXRD solution, a Rietveld refinement was performed on a pXRD pattern of the bulk sample of $LaNiB_3O_7$ synthesized at the stoichiometry described. The model gives an excellent fit to the data with a final composition of 97.5(4) atomic % $LaNiB_3O_7$ and 2.5(1) atomic % LaB_3O_6, with $\chi^2 = 1.88$. It was not possible to obtain a macroscopic sample of polycrystalline $LaNiB_3O_7$ with higher than 98% purity by our methods. The refinement of atomic positions and lattice parameters matches well with the structural solution from the single crystal data. The room-temperature pXRD pattern, calculated pattern, and difference are plotted in **Fig. 3**. As the fraction of LaB_3O_6 impurity was

very small, and the impurity is non-magnetic, magnetic characterization could be performed on the polycrystalline sample.

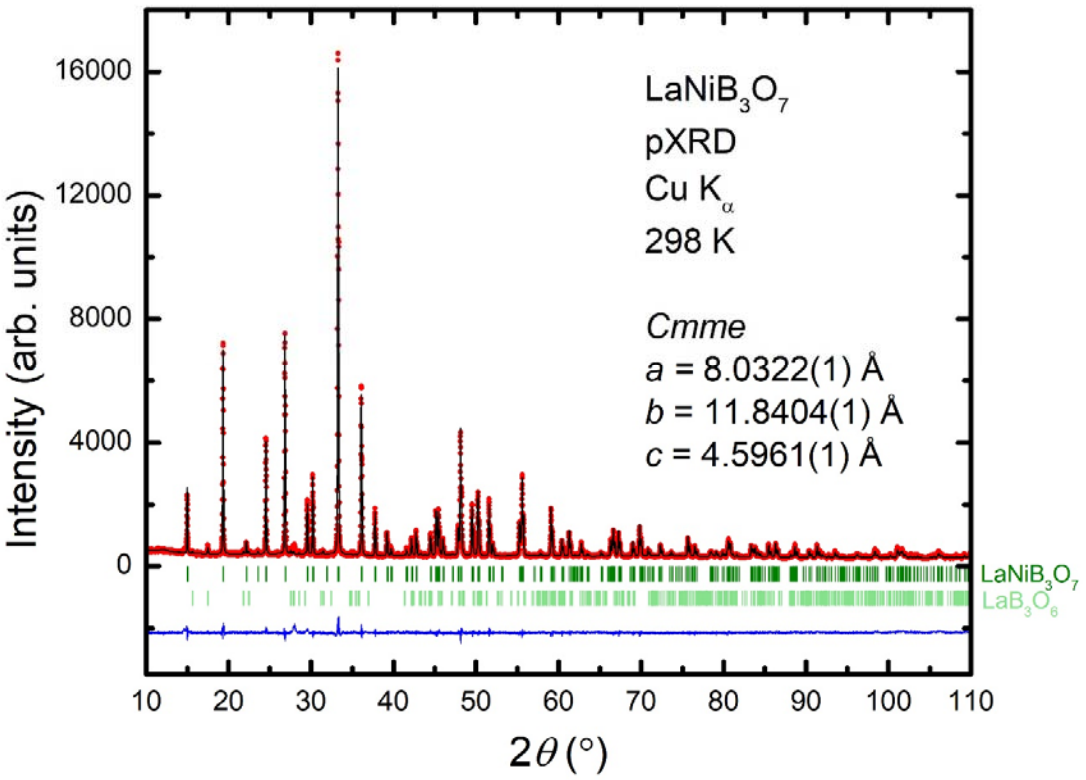

Fig. 3. Room-temperature pXRD pattern of $LaNiB_3O_7$, λ=1.5406 Å. Observed data in red and calculated refinement in black. Bragg reflections are shown in dark green for $LaNiB_3O_7$ (top *hkl* ticks) and in light green for impurity phase LaB_3O_6 (bottom *hkl* ticks). Difference between observed and calculated patterns in blue. Starting from the single crystal parameters, an excellent fit was obtained with χ^2 = 1.88 and R_1(obs) = 0.0117. The fit gave a final composition of 97.5(4) atomic % $LaNiB_3O_7$ and 2.5(1) atomic % LaB_3O_6.

Temperature-dependent zero-field cooled (ZFC) magnetization data were obtained from 1.74 to 300 K with applied fields of 5000 and 3000 Oe. Due to the presence of a small ferromagnetic impurity (not visible by pXRD but common for Ni-containing compounds, as discussed later), we subtracted the magnetization data (*M)* obtained at 3000 Oe from those collected at 5000 Oe and

divided by the difference in field (H) and moles of Ni to obtain the intrinsic molar magnetic susceptibility (χ) [21], which is plotted in **Fig. 4** (*left axis*). The sharp downturn in χ at approximately 19 K is indicative of a transition to an antiferromagnetically ordered state. Slight changes in slope of the susceptibility at approximately 25 and 50 K may indicate more complex magnetic behavior above T_N that may warrant further characterization, but this is beyond the scope of the current work. The inverse ZFC susceptibility, with subtraction of a temperature-independent diamagnetic correction (χ_0 = -0.00174 emu·mol$_{Ni}^{-1}$·Oe^{-1}), is also shown in **Fig. 4** (*right axis*) and has been fit to the Curie-Weiss law. We find the Weiss temperature to be θ_{CW} = -39.5 K, which is consistent with the dominance of antiferromagnetic interactions in our material and the observed T_N, and an effective magnetic moment per Ni of 2.66 μ_B. The expected spin-only value per Ni^{2+} ion is 2.83 μ_B/Ni, within error of the value obtained for $LaNiB_3O_7$.

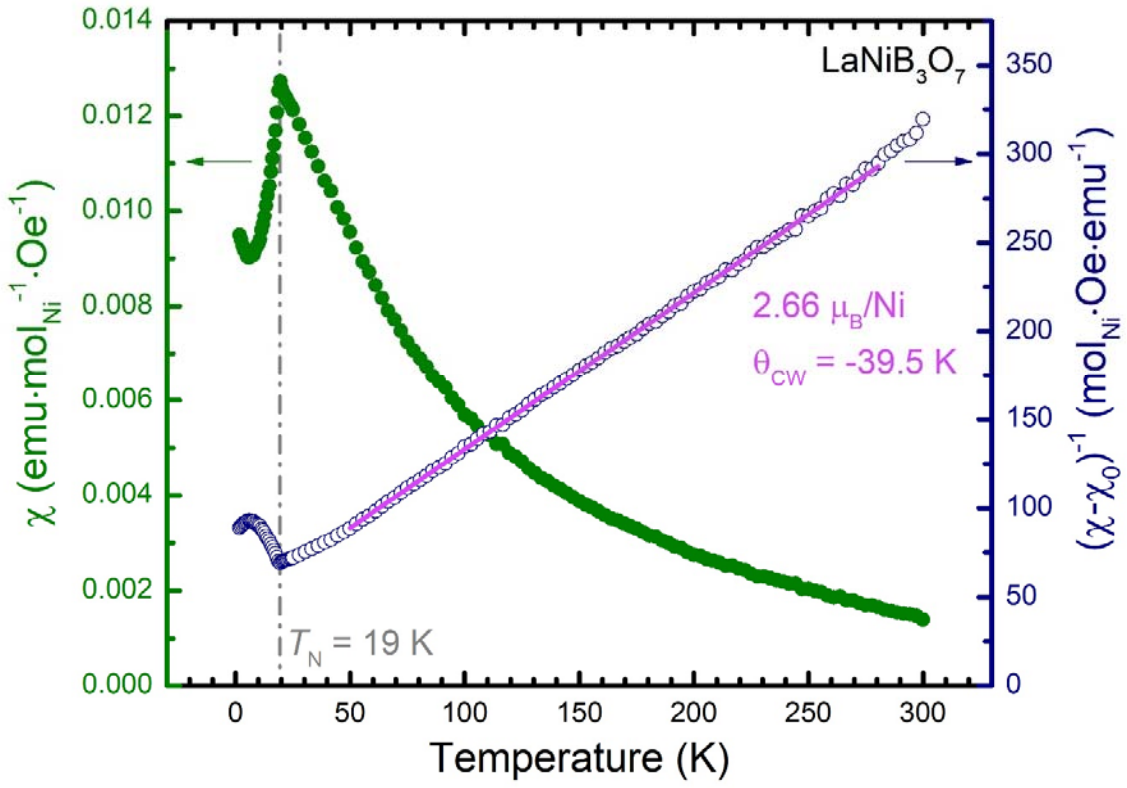

Fig. 4: Zero-field cooled magnetic susceptibility vs. temperature data (green, left axis) obtained from ($M_{5000\ Oe} - M_{3000\ Oe}$)/2000 Oe/$mol_{Ni}$. A downturn at approximately 19 K reveals a transition to an antiferromagnetically ordered state. The inverse χ_0-subtracted susceptibility vs. temperature (unfilled navy circles, right axis, χ_0 = -0.00174 emu·mol_{Ni}^{-1} ·Oe^{-1}) was fit with the Curie Weiss law (pink). This fit gives a Weiss temperature of θ_{CW} = -39.5 K, indicating dominantly antiferromagnetic interactions, and a magnetic moment of 2.66 μ_B/Ni.

We also obtained field-dependent magnetization ($M(H)$) at 1.75, 15, 30, and 150 K as shown in the main panel of **Fig. 5**. The slight ferromagnetic magnetization with hysteresis at low fields in the $M(H)$ data up to 150 K (**Fig. 5**, *inset*) indicates that there is a small elemental Ni impurity present in the sample, one too small to be discernable in the pXRD patterns collected. The magnetic response is linear from 2000 to 5000 Oe at all temperatures measured. Thus, to obtain the intrinsic

magnetic behavior, we subtracted the magnetization obtained at 3000 Oe from that collected at 5000 Oe and divided the result by the difference in field (ie. $\chi = \Delta M/\Delta H$). We note that the Néel ordering transition at 19 K is also clearly visible in the magnetization data measured at H = 5000 and 3000 Oe.

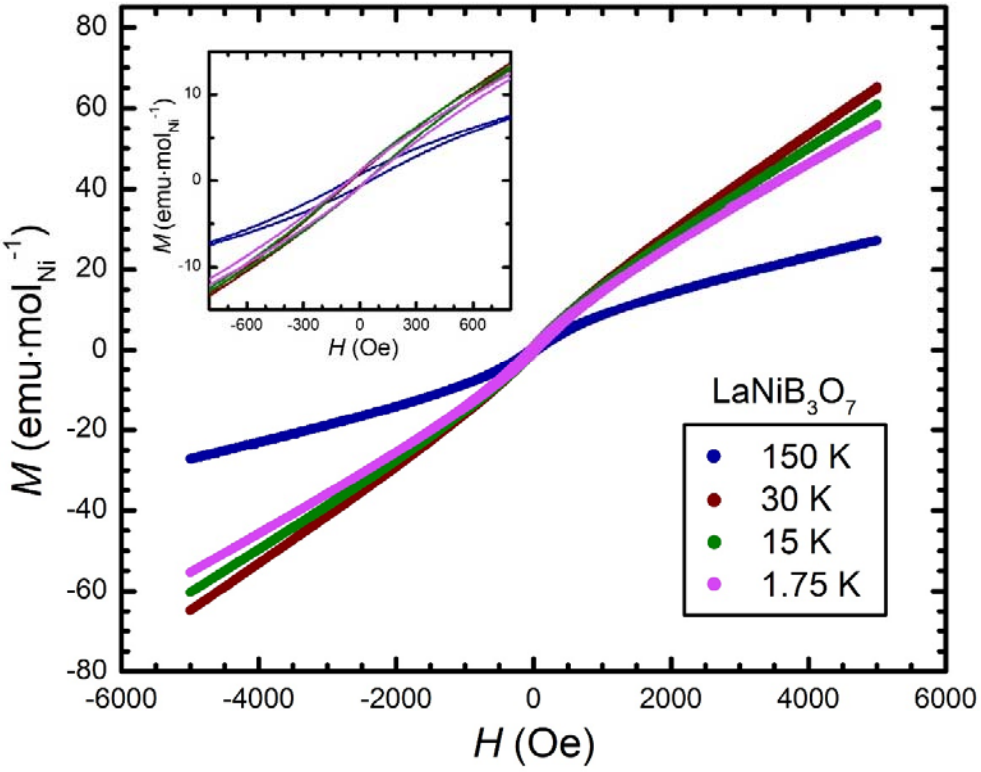

Fig. 5: Magnetization per mol Ni vs. applied field at 1.75 K (pink), 15 K (green), 30 K (red), and 150 K (blue). Magnetic response is shown to be linear from 2000 to 5000 Oe for all temperatures. Inset displays slight hysteresis present at low fields for all temperatures.

The temperature-dependent specific heat was measured from 40 to 1.85 K under zero applied magnetic field for a pressed, annealed pellet of the polycrystalline material (**Fig. 6**). The sharp peak in the specific heat at 19 K indicates a phase transition and corresponds well to the transition

to the antiferromagnetic state observed in the ZFC magnetic susceptibility data. Thus, we confirm the Néel temperature (T_N) of $LaNiB_3O_7$ to be 19 K. If there is a non-magnetic analogue discovered in the future, it would be beneficial to subtract the specific heat of the analogue in order to isolate the magnetic contribution to the specific heat and calculate the magnetic entropy.

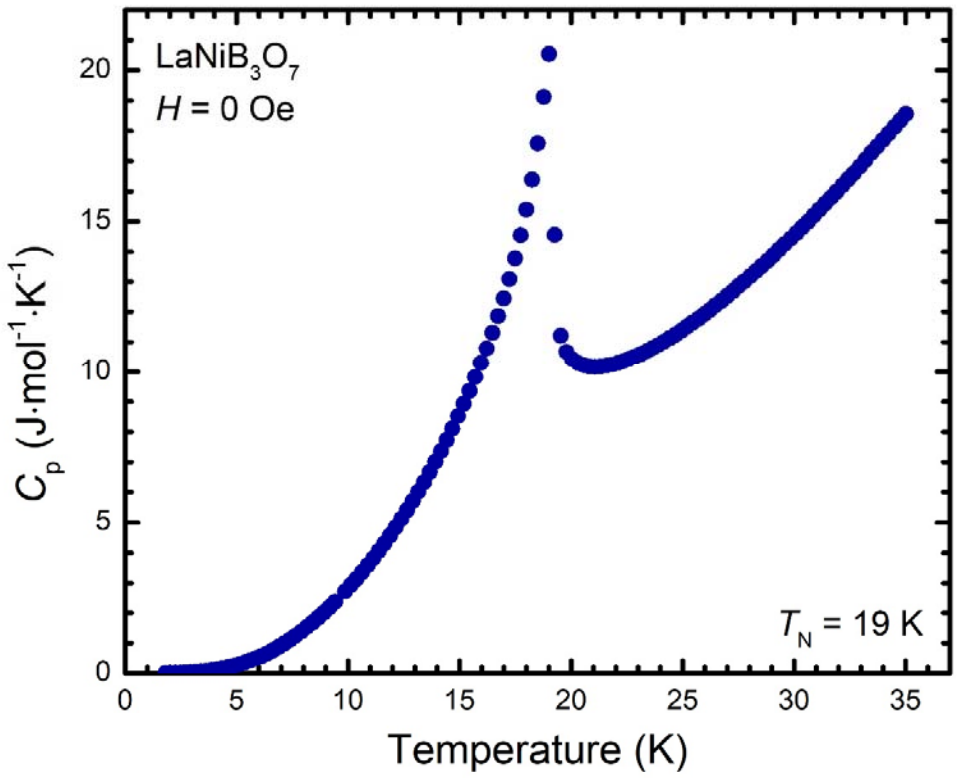

Fig. 6: Temperature-dependent heat capacity data obtained under zero applied magnetic field. The anomaly in the heat capacity, with a peak value of 19 K, matches well with the transition to the antiferromagnetic state observed in the χ vs. T plot. From these data, the Néel temperature can be assigned as T_N = 19 K.

4. Conclusions

In summary, we have presented the structural and magnetic characterization of $LaNiB_3O_7$, an antiferromagnet and the first compound of the $CaAlB_3O_7$ structure type to contain a rare-earth

element or a transition metal, and the first to exhibit magnetic ordering, to the best of our knowledge. Temperature-dependent magnetic susceptibility measurements reveal an antiferromagnetic transition at T_N = 19 K, which specific heat data confirm. Certain features in the magnetic susceptibility data may warrant further magnetic characterization in future work. Our synthesis of $LaNiB_3O_7$ expands the chemistry accessible in this structure type by demonstrating the ability for the AMB_3O_7 lattice to accommodate A^{2+} and M^{3+} ions (as in $CaAlB_3O_7$) or A^{3+} and M^{2+} ions (as in our phase). This greatly expands the synthetic space in the search for new isostructural phases, as various alkaline earth metals or *RE* elements can be substituted on the *A* site, as well as a greater diversity in *TM* oxidation states and, potentially, magnetism of the compounds.

Supporting Information: CSD 1872599 contains the supplementary crystallographic data for this paper. This data can be obtained free of charge via www.ccdc.cam.ac.uk/data_request/cif, or by emailing data_request@ccdc.cam.ac.uk, or by contacting The Cambridge Crystallographic Data Centre, 12 Union Road, Cambridge CB2 1EZ, UK; fax: + 441223336033.

Acknowledgements

The authors thank Tai Kong and Tomasz Klimczuk for their helpful discussions regarding the magnetism and specific heat data. Materials synthesis was supported by the U.S. Department of Energy, Division of Basic Energy Sciences (grant DE-FG02-98ER45706). Structural characterization was supported by the Gordon and Betty Moore Foundation EPiQS initiative (grant GBMF-4412). K.M.P. acknowledges the support of the National Science Foundation Graduate Research Fellowship under Grant No. DGE-1656466.

Declarations of interest

None.

References

[1] I.Z. Gokhman, B.F. Dzhurinskadzhurinsky, B.A. Yefremov, A.B. Ilyukhin, V.I. Chistova, Synthesis and structure of boratotungstates Ln3BWO9 (Ln La, Pr, Nd, Sm-Ho), Zh. Neorg. Khim. 39 (1994) 1075–1079.

[2] S.Y. Stefanovich, N.U. Venskovskii, A.V. Mosunov, V.A. Krut'ko, Optical Nonlinearity and Dielectric Properties of Noncentrosymmetric Crystals of RE Borotungstate Family Ln3BWO9, Russ. J. Inorg. Chem. 46 (2001) 1864–1868.

[3] R. Zhu, Y. Huang, H.J. Seo, A Red-Emitting Phosphor of Eu-Based Borotungstate Eu3BWO9 for White Light-Emitting Diodes, J. Electrochem. Soc. 157 (2010) H1116–H1120. doi:https://doi.org/10.1149/1.3501964.

[4] J.A. Campá, C. Cascales, E. Gutiérrez-Puebla, M.A. Monge, I. Rasines, C. Ruíz-Valero, Crystal Structure, Magnetic Order, and Vibrational Behavior in Iron Rare-Earth Borates, Chem. Mater. 9 (1997) 237–240. doi:10.1021/cm960313m.

[5] Y. Hinatsu, Y. Doi, K. Ito, M. Wakeshima, A. Alemi, Magnetic and calorimetric studies on rare-earth iron borates LnFe3(BO3)4 (Ln=Y, La–Nd, Sm–Ho), J. Solid State Chem. 172 (2003) 438–445. doi:10.1016/S0022-4596(03)00028-8.

[6] E.A. Popova, N. Tristan, C. Hess, R. Klingeler, B. Büchner, L.N. Bezmaternykh, V.L. Temerov, A.N. Vasil'ev, Magnetic and thermal properties of single-crystal NdFe3(BO3)4, J. Exp. Theor. Phys. 105 (2007) 105–107. doi:10.1134/S1063776107070229.

[7] C. Ritter, A. Balaev, A. Vorotynov, G. Petrakovskii, D. Velikanov, V. Temerov, I. Gudim, Magnetic structure, magnetic interactions and metamagnetism in terbium iron borate TbFe3(BO3)4: a neutron diffraction and magnetization study, J. Phys.: Condens. Matter. 19 (2007) 196227. doi:10.1088/0953-8984/19/19/196227.

[8] E.A. Popova, N. Tristan, A.N. Vasiliev, V.L. Temerov, L.N. Bezmaternykh, N. Leps, B. Büchner, R. Klingeler, Magnetization and specific heat of DyFe3(BO3)4 single crystal, Eur. Phys. J. B. 62 (2008) 123–128. doi:10.1140/epjb/e2008-00146-5.

[9] C. Ritter, A. Vorotynov, A. Pankrats, G. Petrakovskii, V. Temerov, I. Gudim, R. Szymczak, Magnetic structure in iron borates RFe $_3$ (BO $_3$) $_4$ (R = Y,Ho): a neutron diffraction and magnetization study, J. Phys.: Condens. Matter. 20 (2008) 365209. doi:10.1088/0953-8984/20/36/365209.

[10] Y. Doi, T. Satou, Y. Hinatsu, Crystal structures and magnetic properties of lanthanide containing borates LnM(BO3)2 (Ln=Y, Ho–Lu; M=Sc, Cr), J. Solid State Chem. 206 (2013) 151–157. doi:10.1016/j.jssc.2013.08.015.

[11] R. Sinclair, H.D. Zhou, M. Lee, E.S. Choi, G. Li, T. Hong, S. Calder, Magnetic ground states and magnetodielectric effect in RCr(BO3)2 (R = Y and Ho), Phys. Rev. B. 95 (2017) 174410. doi:10.1103/PhysRevB.95.174410.
[12] Inorganic Crystal Structure Database (ICSD) Web, Version 3.5.0, FIZ Karlsruhe, Germany, 2017., n.d.
[13] G.M. Sheldrick, SHELXS-97 and SHELXL-97, Program for crystal structure solution and refinement, University of Go:ttingen, Germany, 1997.
[14] O.V. Dolomanov, L.J. Bourhis, R.J. Gildea, J.A.K. Howard, H. Puschmann, OLEX2 : a complete structure solution, refinement and analysis program, J. Appl. Crystallogr. 42 (2009) 339–341. doi:10.1107/S0021889808042726.
[15] A.L. Spek, Single-crystal structure validation with the program PLATON, J. Appl. Crystallogr. 36 (2003) 7–13. doi:10.1107/S0021889802022112.
[16] K. Momma, F. Izumi, VESTA 3 for three-dimensional visualization of crystal, volumetric and morphology data, J. Appl. Crystallogr. 44 (2011) 1272–1276. doi:10.1107/S0021889811038970.
[17] P.B. Moore, T. Araki, Johachidolite, CaAl[B3O7], a Borate with Very Dense Atomic Structure, Nature. 240 (1972) 63–65.
[18] L.F. Aristarain, R.C. Erd, Johachidolite redefined: a calcium aluminum borate, Am. Mineral. 62 (1977) 327–329.
[19] M. Kadiyski, T. Armbruster, D. Günther, E. Reusser, A. Peretti, Johachidolite, CaAl[B3O7], a mineralogical and structural peculiarity, Eur. J. Mineral. 20 (2008) 965–973. doi:10.1127/0935-1221/2008/0020-1824.
[20] K.-I. Machida, G.-Y. Adachi, J. Shiokawa, M. Shimada, M. Koizumi, Structure of strontium tetraaluminate β-SrAl4O7, Acta Crystallogr. B. 38 (1982) 889–891. doi:10.1107/S0567740882004294.
[21] K.L. Holman, E. Morosan, P.A. Casey, L. Li, N.P. Ong, T. Klimczuk, C. Felser, R.J. Cava, Crystal structure and physical properties of Mg6Cu16Si7-type M6Ni16Si7, for M = Mg, Sc, Ti, Nb, and Ta, Mater. Res. Bull. 43 (2008) 9–15. doi:10.1016/j.materresbull.2007.09.023.